

## Review

# $[^{18}\text{F}]$ Tetrafluoroborate ( $[^{18}\text{F}]$ TFB) and its analogs for PET imaging of the sodium/iodide symporter

Huailei Jiang<sup>✉</sup>, Timothy R. DeGrado<sup>✉</sup>

Department of Radiology, Mayo Clinic, Rochester MN USA

✉ Corresponding authors: Dr. Timothy R. DeGrado, Department of Radiology, Mayo Clinic, 200 First St. SW, Rochester, MN 55905. E-mail: degrado.timothy@mayo.edu; Tel: 507-538-4319; FAX: 507-266-4461 and Dr. Huailei Jiang, Department of Radiology, Mayo Clinic, 200 First St. SW, Rochester, MN 55905. E-mail: Jiang.huailei@mayo.edu

© Ivyspring International Publisher. This is an open access article distributed under the terms of the Creative Commons Attribution (CC BY-NC) license (<https://creativecommons.org/licenses/by-nc/4.0/>). See <http://ivyspring.com/terms> for full terms and conditions.

Received: 2018.01.17; Accepted: 2018.03.16; Published: 2018.06.24

## Abstract

Sodium/iodide symporter (NIS)-mediated iodide uptake in thyroid follicular cells is the basis of clinical utilization of radioiodines. The cloning of the NIS gene enabled applications of NIS as a reporter gene in both preclinical and translational research. Non-invasive NIS imaging with radioactive iodides and iodide analogs has gained much interest in recent years for evaluation of thyroid cancer and NIS reporter expression. Although radioiodines and  $[^{99\text{m}}\text{Tc}]$ pertechnetate ( $[^{99\text{m}}\text{Tc}]\text{TcO}_4^-$ ) have been utilized in positron emission tomography (PET) and single photon emission computed tomography (SPECT), they may suffer from limitations of availability, undesirable decay properties or imaging sensitivity (SPECT versus PET). Recently,  $[^{18}\text{F}]$ tetrafluoroborate ( $[^{18}\text{F}]$ TFB or  $[^{18}\text{F}]\text{BF}_4^-$ ) and other fluorine-18 labeled iodide analogs have emerged as a promising iodide analog for PET imaging. These fluorine-18 labeled probes have practical radiosyntheses and biochemical properties that allow them to closely mimic iodide transport by NIS in thyroid, as well as in other NIS-expressing tissues. Unlike radioiodides, they do not undergo organification in thyroid cells, which results in an advantage of relatively lower uptake in normal thyroid tissue. Initial clinical trials of  $[^{18}\text{F}]$ TFB have been completed in healthy human subjects and thyroid cancer patients. The excellent imaging properties of  $[^{18}\text{F}]$ TFB for evaluation of NIS-expressing tissues indicate its bright future in PET NIS imaging. This review focuses on the recent evolution of  $[^{18}\text{F}]$ TFB and other iodide analogs and their potential value in research and clinical practice.

Key words: sodium/iodide symporter, positron emission tomography, radioiodine,  $[^{18}\text{F}]$ tetrafluoroborate, radiochemistry, molecular imaging

## 1. Introduction

Iodine is an essential element in thyroid physiology and the accumulation of iodine in the thyroid was found to be a critical step for the synthesis of thyroid hormones as early as 1915. For over a half century, radioiodines have been successfully used in diagnosis and therapy of thyroid disorders such as hyperthyroidism and thyroid cancer [1-3]. Despite advancement in newer targeted therapies, the clinical utilization of radioiodines remains robust in therapeutic management of thyroid function and monitoring outcomes of treatment [4-8].

The mechanism of iodide uptake was not fully elucidated until the NIS gene was cloned in 1996 [9, 10]. This work tremendously improved the understanding of thyroid physiology and enabled new approaches for molecular imaging and treatment [4, 5, 11-14]. Due to the broad availability of SPECT and PET scanners and iodide radiopharmaceuticals ( $[^{123/124/131}\text{I}]\text{I}^-$  and  $[^{99\text{m}}\text{Tc}]\text{TcO}_4^-$ ), NIS has been developed as an imaging reporter gene with great promise for clinical translation [15-18]. Despite the success of  $[^{99\text{m}}\text{Tc}]\text{TcO}_4^-$  and radioiodides for use in NIS

imaging, there are certain limitations in availability and physical properties of these radioisotopes. These limitations have been largely addressed by the recent development of [<sup>18</sup>F]TFB for NIS imaging using PET [19]. Initial clinical trials of [<sup>18</sup>F]TFB have been completed in healthy human subject [20] and thyroid cancer patients [21, 22]. This review focuses on the development of [<sup>18</sup>F]TFB and closely related compounds as iodide analogs for PET imaging of NIS expression in tissues.

## 2. Noninvasive imaging of NIS

There are a few techniques available for NIS expression monitoring. Currently, SPECT and PET offer the best sensitivity in NIS imaging [23, 24]. Moreover, the integration of SPECT or PET and computed tomography (CT) allows the combination of functional data with detailed anatomical images to generate more accurate localization and quantitative estimated radioactivity concentrations in live subjects [25, 26]. Several iodide radionuclides have been used for noninvasive imaging of NIS expression using SPECT and PET modalities (Table 1).

**Table 1.** Radionuclides for SPECT and PET imaging of NIS.

Radionuclides	T <sub>1/2</sub>	Decay properties	Availability	Application
Technetium-99m	6 h	γ: 98.6% (141 keV)	Reactor/Generator	SPECT
Iodine-123	13.3 h	γ: 83.3% (159 keV)	Specific cyclotron	SPECT
Iodine-131	8 d	β <sup>-</sup> : 89.9% (606 keV) γ: 81.7% (364 keV)	Specific cyclotron	SPECT/ therapy
Iodine-125	59 d	γ: 6.5% (35 keV)	Specific cyclotron	Small animal SPECT
Iodine-124	4.2 d	β <sup>-</sup> : 23% (1543, 2146 keV), γ: 11-63% (0.6-1.7 MeV)	Specific cyclotron	PET
Fluorine-18	109.8 min	β <sup>+</sup> : 97% (634 keV)	Most medical cyclotron/accelerators	PET

### 2.1. SPECT imaging of NIS

SPECT is a useful noninvasive imaging technique. Three-dimensional images are obtained by detecting photons emitted from a radionuclide [27], e.g., technetium-99m or iodine-123/125/131. Technetium-99m has a half-life of 6 h and high abundance of photon emission with desirable energy (98.6%, 141 keV) for medical diagnostic imaging [28, 29]. The anion [<sup>99m</sup>Tc]TcO<sub>4</sub><sup>-</sup> is a good transport substrate for NIS and therefore is useful for NIS imaging using SPECT [15]. Technetium-99m is the daughter product of molybdenum-99 [30], and is usually eluted from a generator. However, the global shortage of technetium-99m has bothered the medical imaging field in the last two decades due to the fragile supply chain of molybdenum-99 [31-33]. Iodine-123 is the most suitable radioiodine for SPECT imaging of NIS [34-36]. Iodine-123 has a half-life of 13.3 h and

83.3% emitted photon with predominant energy of 159 keV, which is close to technetium-99m [37]. Iodine-123 provides higher sensitivity and imaging quality compared to iodine-125/131. Iodine-125 has limited use in SPECT because of its rather low photon energy (35 keV) and undesirable long half-life (59 d) [38]. [<sup>131</sup>I]I<sup>-</sup> can be used as both diagnostic and therapeutic agent [39-41]. Iodine-131 has a half-life of 8 days with two step emission of beta particles (89%, 606 keV) and photon emission (81%, 364 keV), which is too high for optimal imaging with poor quality. The long half-lives of radioiodine in diagnostic imaging resulted in extra exposure for both patient and staff. Meanwhile, all the radioiodides [<sup>123/125/131</sup>I]I<sup>-</sup> have limitations of availability due to the requirement of specialized production systems [42], which are only available in limited sites.

### 2.2. PET imaging of NIS

#### 2.2.1. PET imaging of NIS using [<sup>124</sup>I]iodide

PET is a highly sensitive noninvasive imaging technique that utilizes positron-emitting radiopharmaceuticals. Three-dimensional images are reconstructed from detected pairs of photons (511 keV) emitted upon annihilation of positrons with electrons in tissue. Currently, PET imaging offers the highest imaging sensitivity for detecting low levels of reporter gene expression. Iodine-124 is a positron-emitting radionuclide [43] that has been used for NIS imaging using PET and has the advantages of superior quantitation and imaging sensitivity of PET relative to SPECT [44]. However, iodine-124 suffers several drawbacks [45]: 1) its 4.2 d half-life and low positron yield are undesirable for diagnostic imaging as these result in high radiation exposures; 2) its high energy single photon emissions (0.6-1.7 MeV) can degrade image quality; and 3) its high positron emission energy results in >6 mm maximum travel in tissue before annihilation [15], which degrades imaging resolution.

#### 2.2.2. [<sup>18</sup>F]TFB provides a new approach for NIS imaging with PET

Fluorine-18 is the radionuclide of choice for clinical PET studies [46]. It has a high positron emission yield (98%) and relatively low energy (0.64 MeV), providing a limited maximum distance travelled in tissue before annihilation, which gives excellent resolution. Its half-life of 109.8 min is compatible with typical imaging period, resulting in acceptable radiation exposure levels. Moreover, due to the widespread use of [<sup>18</sup>F]FDG, fluorine-18 is routinely available in most medical cyclotron centers and PET radiopharmaceutical distribution companies. Therefore, a fluorine-18-based radiotracer for NIS

imaging would have great value to overcome many of the limitations of traditional radioiodine and technetium-99m tracers.  $[^{18}\text{F}]\text{TfB}$  has emerged as a promising iodide analog radiotracer for NIS imaging. The tetrafluoroborate (TFB) anion is an analog of iodide with good relative stability under physiological conditions and low toxicity. As early as the 1950's, Anbar et al. [47-49] reported the radiolabeling of  $[^{18}\text{F}]\text{TfB}$  by isotopic exchange using reactor-generated  $[^{18}\text{F}]\text{fluoride}$  on nonradioactive TFB under acidic conditions, and performed in vitro evaluations of competitive binding with other iodide analogs in the early 1960's. Despite the low molar activities obtained in the synthesis,  $[^{18}\text{F}]\text{TfB}$  showed specific accumulation in thyroid and high thyroid-to-blood concentration ratio. This pioneering study suggested its potential for thyroid imaging. However, these studies were done three decades before the advent of clinical PET and even longer before characterization and use of hNIS as gene reporter. Due to the utility of radioiodines and  $[^{99\text{m}}\text{Tc}]\text{TcO}_4^-$  in imaging of NIS with SPECT,  $[^{18}\text{F}]\text{TfB}$  was inactive in the literature for half a century despite of its potential. **Figure 1** shows a timeline of the inception and development of  $[^{18}\text{F}]\text{TfB}$  as a radiotracer for PET imaging of NIS. The synthesis methods (section 3) and biological evaluation studies (sections 4-5) for  $[^{18}\text{F}]\text{TfB}$  will be reviewed in detail below.

### 2.2.3. Other fluorine-18 labeled iodide analogs

Due to the encouraging experience on NIS imaging with  $[^{18}\text{F}]\text{TfB}$ , other promising fluorine-

containing iodide analogs have been explored as potential fluorine-18 labeled NIS probes.  $[^{18}\text{F}]\text{fluorosulfate}$  ( $[^{18}\text{F}]\text{FSO}_3^-$ ) was obtained in high radiochemical yield and molar activity, and has a similar affinity with  $[^{18}\text{F}]\text{TfB}$  in a NIS-mediated competitive uptake assay [50]. Meanwhile, the hexafluorophosphate ( $\text{PF}_6^-$ ) ion has been shown the highest known affinity as an inhibitor for NIS transport [50, 51]. More details about the radiochemistry and biological evaluation of these newer fluorine-18 labeled probes will be described in the following sections.

## 3.0. Synthesis of fluorine-18 labeled iodide analogs

### 3.1. Radiosynthesis of $[^{18}\text{F}]\text{TfB}$

#### 3.1.1. Isotope-exchange labeling

In 2010, Jauregui-Osoro et al. [19] updated the isotope exchange radiolabeling of  $[^{18}\text{F}]\text{TfB}$  with modern production of  $[^{18}\text{F}]\text{fluoride}$  using a low energy cyclotron (**Figure 2**).  $[^{18}\text{F}]\text{TfB}$  was conveniently purified with a disposable silver ion-loaded cation exchange cartridge and two alumina N cartridges, and the quality control was performed by thin-layer chromatography and anion HPLC. Using this simple and practical production method, the molar activity of  $[^{18}\text{F}]\text{TfB}$  reported by Jauregui-Osoro was up to 1 GBq/ $\mu\text{mol}$  with a starting activity of 12-18 GBq, which is moderate with respect to molar activities commonly required for receptor-binding radiopharmaceuticals [52]. Also, the 10% radiochemical yield was rather low.

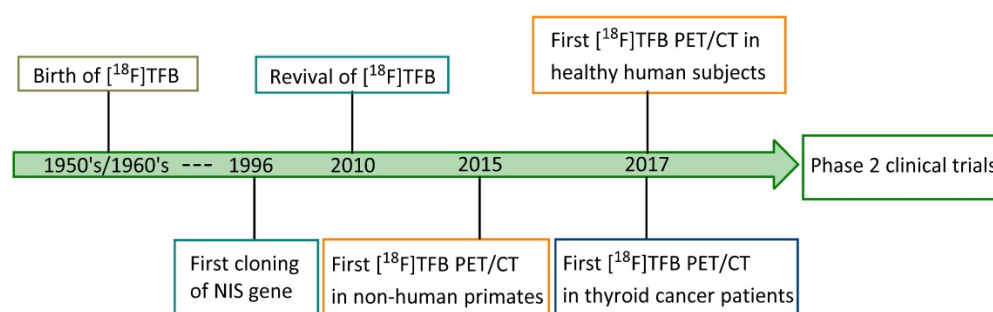


**Figure 1.** Timeline of advancements in  $[^{18}\text{F}]\text{TfB}$  NIS imaging: 1950's to date.

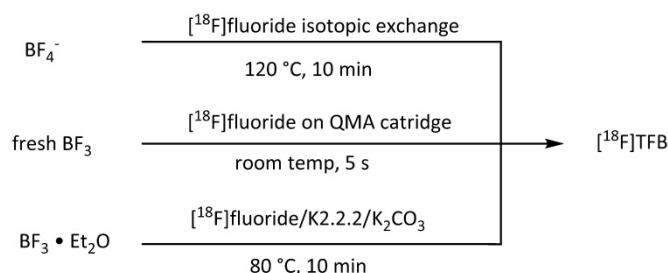


**Figure 2.** Radiosynthesis of  $[^{18}\text{F}]\text{TfB}$ . QMA: quaternary methyl ammonium. K.2.2.2: Kryptofix® 2.2.2.

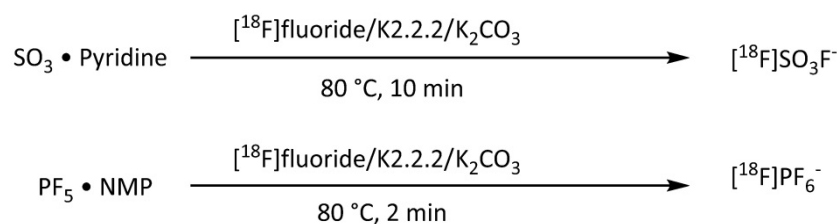


**Figure 3.** Radiosynthesis of [<sup>18</sup>F]fluorosulfate and [<sup>18</sup>F]hexafluorophosphate.

### 3.1.2. Radiofluorination of BF<sub>3</sub>

To achieve higher molar activities of [<sup>18</sup>F]TFB, Jiang et al. [53] developed a novel approach of [<sup>18</sup>F]TFB production using fresh boron trifluoride (BF<sub>3</sub>) (formulated in petroleum ether/tetrahydrofuran 50:1) solution, which was highly reactive with [<sup>18</sup>F]fluoride (Figure 2). This method allowed a fast formation of [<sup>18</sup>F]TFB upon passing the BF<sub>3</sub> solution at room temperature through a quaternary methyl ammonium (QMA) cartridge containing trapped [<sup>18</sup>F]fluoride. Molar activity of [<sup>18</sup>F]TFB of 8.84±0.56 GBq/μmol and radiochemical yield of 20.0±0.7% were obtained with starting activity of 40-44 GBq. Due to the convenient and fast radiofluorination, [<sup>18</sup>F]TFB was obtained in an overall synthesis time of 10 min. Meanwhile, Khoshnevisan et al. [54] and Volpe et al. [55] reported another approach for synthesis of higher molar activity of [<sup>18</sup>F]TFB utilizing BF<sub>3</sub> as precursor. In their synthesis, the [<sup>18</sup>F]fluoride starting reagent was in the form of azeotropically dried [<sup>18</sup>F]KF/K<sub>2</sub>CO<sub>3</sub> and the BF<sub>3</sub> was in the form of commercially available BF<sub>3</sub>•Et<sub>2</sub>O. The reaction was performed for 10 min at 80 °C. They significantly increased the molar activity of [<sup>18</sup>F]TFB to 5.7±3.5 GBq/μmol with decay corrected radiochemical yields of 13.2±5.9% from a starting activity of 1.5 GBq.

All the reported methods for production of [<sup>18</sup>F]TFB are summarized in Table 2. The improved methodologies for [<sup>18</sup>F]TFB synthesis based on BF<sub>3</sub> precursor had increased molar activity of [<sup>18</sup>F]TFB and improved radiochemical yield relative to the isotope-exchange method. It is worthy to mention that all the three approaches are compatible for automation and Good Manufacturing Practices (GMP). However, effects of NIS transport saturation with unlabeled TFB present in [<sup>18</sup>F]TFB preparations have been observed in in vitro and small animal in vivo studies [19, 52-54, 56].

**Table 2.** Summary of [<sup>18</sup>F]TFB radiosynthesis methods.

Method	Precursor	Reaction conditions	Non-decay-corrected radiochemical yield	Overall production time	Molar activity at EOS (GBq/μmol)	Starting activity (GBq)	Reference
Isotopic exchange	NaBF <sub>4</sub>	120 °C, 20 min	10%	30 min	1	12-18	[19]
Radiofluorination of BF <sub>3</sub>	Fresh BF <sub>3</sub>	room temp, 5 s	20.0±0.7%	10 min	8.84±0.56	40-44	[53]
	BF <sub>3</sub> •Et <sub>2</sub> O	80 °C, 10 min	13.2±5.9% <sup>a</sup>	39 min	5.7±3.5	1.5	[54]

<sup>a</sup>decay corrected. EOS: end of synthesis

### 3.2. Radiosynthesis of [<sup>18</sup>F]fluorosulfate and [<sup>18</sup>F]hexafluorophosphate

As shown in Figure 3, two additional fluorine-18 based iodide analogs were synthesized recently. Khoshnevisan et al. [50] reported the synthesis of [<sup>18</sup>F]fluorosulfate ([<sup>18</sup>F]FSO<sub>3</sub><sup>-</sup>) ion obtained upon heating of SO<sub>3</sub>-pyridine complex with dried [<sup>18</sup>F]KF/K<sub>2</sub>.2.2/K<sub>2</sub>CO<sub>3</sub>. Excellent molar activity of ≥48.5 GBq/μmol and radiochemical yield of 31.6% were obtained starting with 750 MBq of [<sup>18</sup>F]fluoride. Jiang et al. [57] developed a synthesis of [<sup>18</sup>F]hexafluorophosphate ([<sup>18</sup>F]HFP) based on the radiofluorination of PF<sub>5</sub>/N-Methyl-2-pyrrolidone (PF<sub>5</sub>•NMP) complex with [<sup>18</sup>F]KF/K<sub>2</sub>.2.2/K<sub>2</sub>CO<sub>3</sub>. Due to the high reactivity of PF<sub>5</sub> (even in the presence of NMP), it is likely that hydrolysis leads to moderate levels of [<sup>18</sup>F]HFP molar activity of 604±18 MBq/μmol and low radiochemical yield (10±5%).

## 4. Preclinical imaging studies

### 4.1. Preclinical PET imaging in mice

#### 4.1.1. Normal mice

Using isotope-exchange labeled [<sup>18</sup>F]TFB, Jauregui-Osoro et al. [19] reported in vitro uptake in NIS-expressing FRTL-5 rat thyroid cell lines and PET imaging in BALD/c mice (Figure 4). NIS-specific accumulation of [<sup>18</sup>F]TFB was observed in NIS-expressing cells and tissues. Despite moderate levels of molar activity, high thyroid uptakes and excellent target-to-background resolution were seen in PET images. The preliminary biological evaluation of [<sup>18</sup>F]TFB showed that it has a very similar behavior to [<sup>99m</sup>Tc]TcO<sub>4</sub><sup>-</sup>, which justified its further preclinical and clinical evaluation.

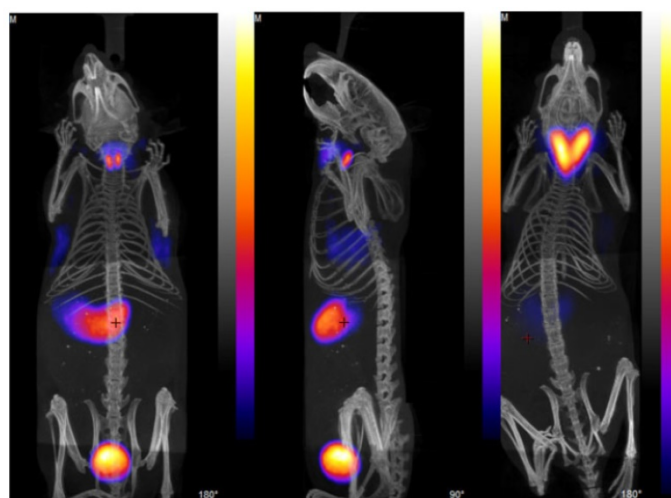


**Figure 4.** PET/CT images with [ $^{18}\text{F}$ ]TFB in mice. (Left) Left and center anterior and (center) lateral view maximum intensity projections of normal mouse 30 min after injection of [ $^{18}\text{F}$ ]TFB. (Right) PET/CT image of TR $\beta$ PV/PV transgenic mouse with thyroid tumor, 30 min after injection with [ $^{18}\text{F}$ ]TFB. Reproduced with permission from [19], copyright 2010 Springer.

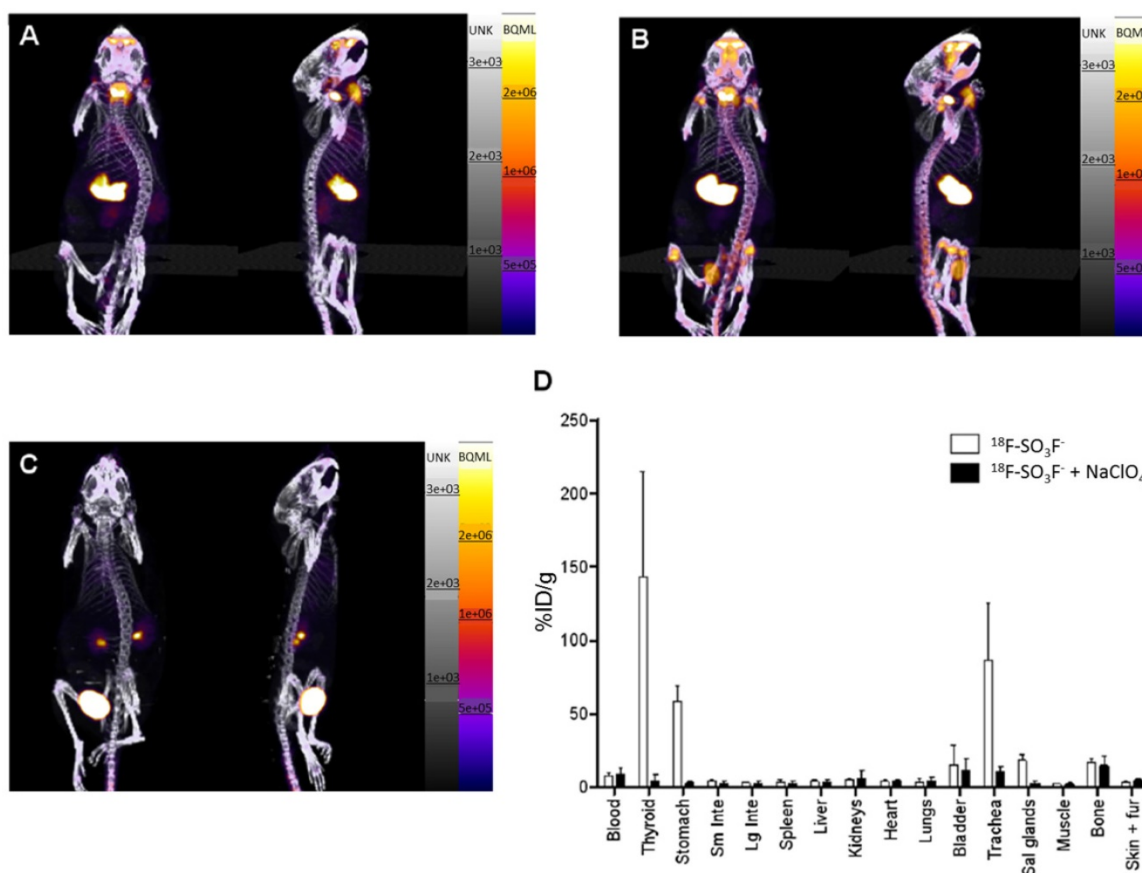


**Figure 5.** (A-C) PET/CT maximum-intensity projections of BALB/c mice. (A) 25-30 min after injection of [ $^{18}\text{F}$ ]SO $_3\text{F}^-$  without perchlorate; (B) 90-120 min after injection of [ $^{18}\text{F}$ ]SO $_3\text{F}^-$  without perchlorate; (C) 25-30 min after injection of [ $^{18}\text{F}$ ]SO $_3\text{F}^-$  in presence of NaClO $_4$  (250 mg/kg). (D) Ex vivo biodistribution data at 2.25 h after injection (n = 3). Error bars represent SD. Reproduced with permission from [50], copyright 2016 Society of Nuclear Medicine and Molecular Imaging, Inc.

Khoshnevisan et al. [50] investigated NIS-mediated [ $^{18}\text{F}$ ]FSO $_3^-$  uptake in cultured NIS-expressing cancer cells and in vivo biodistribution in normal BALB/c mice (Figure 5). [ $^{18}\text{F}$ ]FSO $_3^-$  exhibited a comparable affinity with [ $^{18}\text{F}$ ]TFB in a competitive binding assays using hNIS-transduced HCT116-C19 cells, and showed a

promising specific uptake in NIS expressing tissues in PET/CT imaging and biodistribution. Although the high molar activity [ $^{18}\text{F}$ ]FSO $_3^-$  could greatly avoid the saturable effect in NIS imaging, a moderate amount of bone uptake was also observed, indicating in vivo defluorination of the probe.

#### 4.1.2. NIS gene reporter imaging in mice

As a promising NIS probe, [ $^{18}\text{F}$ ]TFB has been evaluated as a gene reporter probe for monitoring of NIS expression in several approaches where the NIS gene is transfected or transduced into living cells. Weeks et al. [56] evaluated the affinity of [ $^{18}\text{F}$ ]TFB accumulation in a transfected human colon cell line with a stable constitutive expression of functional hNIS (HCT116-hNIS-C19). [ $^{18}\text{F}$ ]TFB accumulation in HCT116-hNIS-C19 cells (31%) was comparable to that of [ $^{188}\text{Re}$ ]perrhenate (41%) and [ $^{99\text{m}}\text{Tc}$ ]TcO $_4^-$  (46%).

Jiang et al. [53] reported [ $^{18}\text{F}$ ]TFB PET imaging in mice bearing NIS-expressing C6 glioma xenografts, with NIS-positive and NIS-negative tumors implanted on opposite flanks (**Figure 6**). In the PET images, high contrast was observed in the uptake of NIS positive tumor over that of NIS negative tumor. [ $^{18}\text{F}$ ]TFB uptake was found to decrease in iodide-accumulating tissues in mice as a function of molar activity (**Figure 6C-E**). Stomach uptake was independent of molar activity of [ $^{18}\text{F}$ ]TFB whereas uptake in hNIS-expressing tumor and thyroid were decreased with decreasing molar activity of [ $^{18}\text{F}$ ]TFB. The uptake of [ $^{18}\text{F}$ ]TFB in hNIS expressing C6 tumor showed dependence on molar activity at 10–0.5 mg of TFB/kg of mouse weight or 0–10 MBq/ $\mu\text{mol}$ ,

considering  $\sim 1.1$  MBq radioactivity was injected in  $\sim 25$  g mice. But this trend was not observed for higher molar activities ( $>10$  MBq/ $\mu\text{mol}$  TFB or  $<0.5$  mg TFB/kg mouse weight). At these higher molar activities, the uptake of [ $^{18}\text{F}$ ]TFB was no longer dependent on molar activity but exhibited high variability, possibly due to variable NIS-expression in the tumors. These results were consistent with the observations of Khoshnevisan et al. [54] on the dependence of [ $^{18}\text{F}$ ]TFB uptake by thyroid on molar activity in normal mice.

Jiang et al. [57] also investigated [ $^{18}\text{F}$ ]HFP with in vivo PET imaging (**Figure 7**) and biodistribution in a C6 glioma xenograft mouse model. [ $^{18}\text{F}$ ]HFP showed robust uptake in NIS-expressing tissues and good in vivo stability. Despite the moderate molar activity of [ $^{18}\text{F}$ ]HFP, the specific accumulation in hNIS-expressing xenograft (hNIS+) was observed clearly relative to isogenic control tumor (hNIS-). The uptake of [ $^{18}\text{F}$ ]HFP in NIS-expressing tissues was successfully blocked by the pretreatment of NaClO $_4$ . It was postulated that the 14–150-fold higher affinity [50] of the PF $_6^-$  relative to endogenous iodide or other endogenous NIS substrates may render [ $^{18}\text{F}$ ]HFP less sensitive to competition effects by other anions in the body.

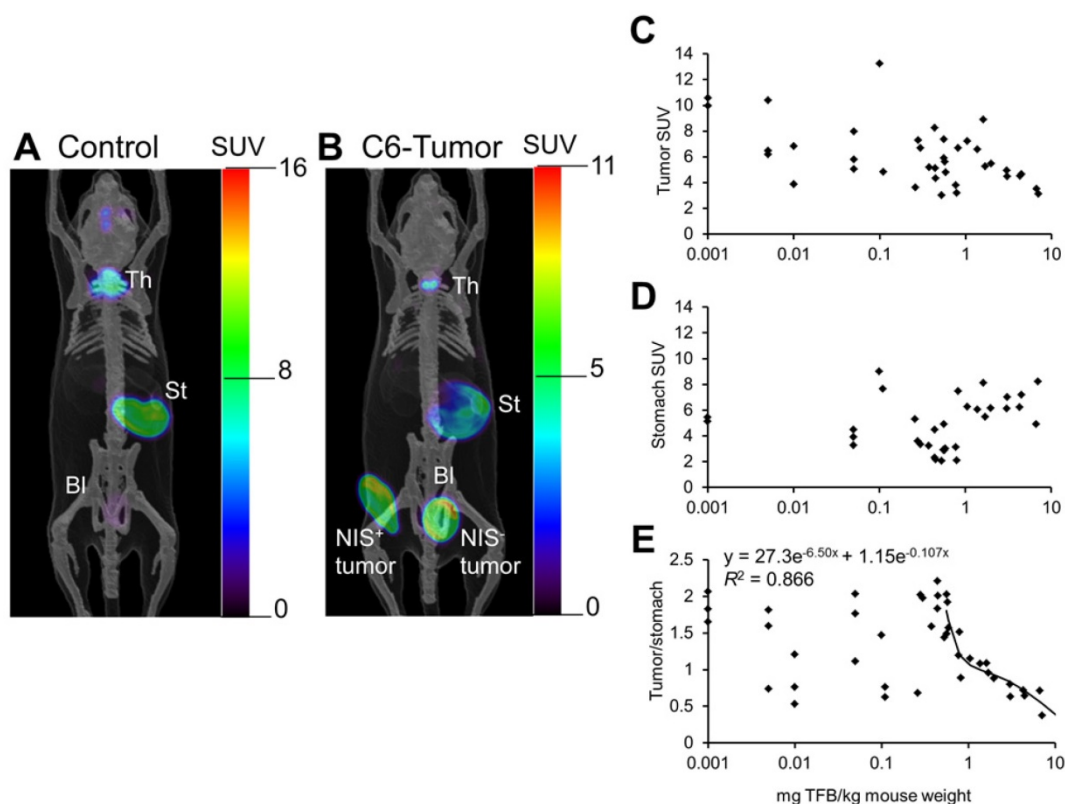


**Figure 6.** PET images of [ $^{18}\text{F}$ ]TFB distribution at 60–70 min in (A) control mouse and (B) mouse bearing hNIS-positive and hNIS-negative C6-glioma xenografts. Overlaid reference bone atlas is computer generated. Bl: bladder; St: stomach; Th: thyroid. Dependence of (C) tumor, (D) stomach, and (E) tumor-to-stomach ratio of [ $^{18}\text{F}$ ]TFB uptake at 60–70 min on administered mass of TFB to hNIS-expressing C6-glioma xenografted mice. Tumor-to-stomach ratio data for administered mass greater than 0.5 mg/kg was fit to a biexponential clearance model using nonlinear least-squares regression. Reproduced with permission from [53], copyright 2016 Society of Nuclear Medicine and Molecular Imaging, Inc.

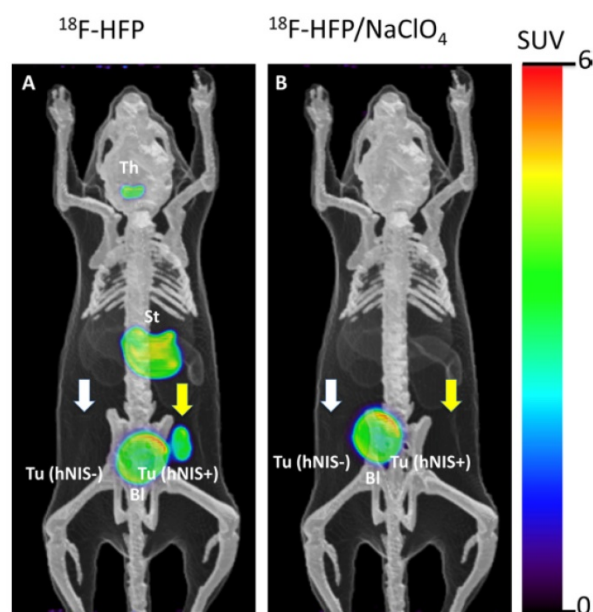


**Figure 7.** Representative PET images of  $[^{18}\text{F}]\text{HFP}$  at 50-60 min post-injection in a mouse bearing hNIS+ and hNIS- C6-glioma xenografts. The overlaid reference bone atlas is computer generated. **(A)**  $[^{18}\text{F}]\text{HFP}$  in unblocked mouse; **(B)**  $[^{18}\text{F}]\text{HFP}$  with pretreatment of  $\text{NaClO}_4$  (250 mg/kg). Th: thyroid, St: stomach, Bl: bladder. Yellow arrows designate the location of hNIS+ tumor. White arrows designate location of hNIS- tumors without detectable uptake of  $[^{18}\text{F}]\text{HFP}$ . Reproduced with permission from [57], copyright 2018 Elsevier.

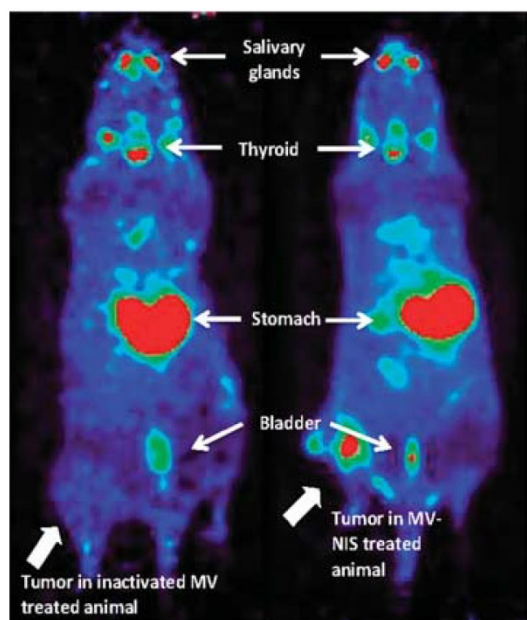


**Figure 8.** Measles virus-expressing NIS (MV-NIS) treatment allows real-time in vivo imaging of viral replication. After 2 weeks of MV-NIS therapy, osteosarcoma xenografts were imaged by PET/CT after  $[^{18}\text{F}]\text{TfB}$  administration. In contrast to MV-NIS-treated animals (right panel), no significant uptake was seen in control virus-treated mice (left panel). Reproduced with permission from [58], copyright 2014 Springer.

Domingo-Musibay et al. [58] reported the use of  $[^{18}\text{F}]\text{TfB}$  in the monitoring NIS reporter gene virotherapy (**Figure 8**). To evaluate the antitumor efficacy of virotherapy with engineered measles virus (MV) NIS-expressing (MV-NIS) vaccine strains for the treatment of osteosarcoma. The  $[^{18}\text{F}]\text{TfB}$  uptake was clearly observed in active MV-NIS-infected tumors in

contrast to tumors treated with inactive virus on PET/CT imaging. Based on these encouraging results,  $[^{18}\text{F}]\text{TfB}$  imaging of NIS reporter gene is warranted in further preclinical and clinical virotherapy studies.

#### 4.1.3. $[^{18}\text{F}]\text{TfB}$ imaging for cell tracking in mice

NIS has been used as a reporter gene in cell tracking studies, which was successfully monitored by iodine-124 PET imaging [59]. Based on their previous work, Lee et al. [60] explored  $[^{18}\text{F}]\text{TfB}$  PET imaging in the tracking of dendritic cell (DC) migration by transfection of murine DC cell lines with hNIS and efflux genes (the latter were monitored by bioluminescence imaging). To monitor the migration of DC cells toward draining popliteal lymph nodes (DPLNs), parental cells were subcutaneously injected into footpads. Immigration of DCs to lymph nodes was successfully monitored using  $[^{18}\text{F}]\text{TfB}$  PET/CT at day 2 imaging and the results were consistent with bioluminescence imaging (**Figure 9**). These data supported the feasibility of using  $[^{18}\text{F}]\text{TfB}$  for hNIS reporter gene imaging to track the migration of DCs to lymph nodes. In this study,  $1 \times 10^7$  cells were contained in the injectate administered to the footpads. Thus, this study begins to provide data on the limits of sensitivity of the  $[^{18}\text{F}]\text{TfB}$  in the application for reporter gene imaging. The ability to monitor NIS expression by PET is likely dependent on a number of factors, including tissue perfusion, density of NIS-expressing cells in target tissue, expression levels of NIS within the cells, molar activity of radiotracer, presence of competing substrates, injected dose, uptake of radiotracer in surrounding background tissues and imaging characteristics of the PET scanner.

Preclinical imaging studies using cancer cells engineered to express reporter genes can provide valuable information on the regional and temporal aspects of tumor metastasis. Diocou et al. [61] recently reported the use of  $[^{18}\text{F}]\text{TfB}$  for metastasis detection in a NIS-expressing orthotopic xenograft breast cancer model (**Figure 10**). Conventional radiotracer  $[^{123}\text{I}]\text{iodide}$  (SPECT/CT) and  $[^{18}\text{F}]\text{FDG}$  were used to compare with  $[^{18}\text{F}]\text{TfB}$  PET/CT imaging.  $[^{18}\text{F}]\text{TfB}$  exhibited high specific uptake in tissues with cancer cell presence. Superior imaging properties for  $[^{18}\text{F}]\text{TfB}$  PET/CT and higher tumor: blood ratios were found relative to  $[^{123}\text{I}]\text{iodide}$  SPECT/CT due to faster blood clearance of  $[^{18}\text{F}]\text{TfB}$  and the inherently higher imaging sensitivity of PET.  $[^{18}\text{F}]\text{FDG}$  PET was unable to differentiate the metastases due to low uptake and poor contrast from adjacent metabolically active tissues. The promising properties of  $[^{18}\text{F}]\text{TfB}$  as gene reporter probe warrant further investigation of  $[^{18}\text{F}]\text{TfB}$  in both preclinical and translational studies.

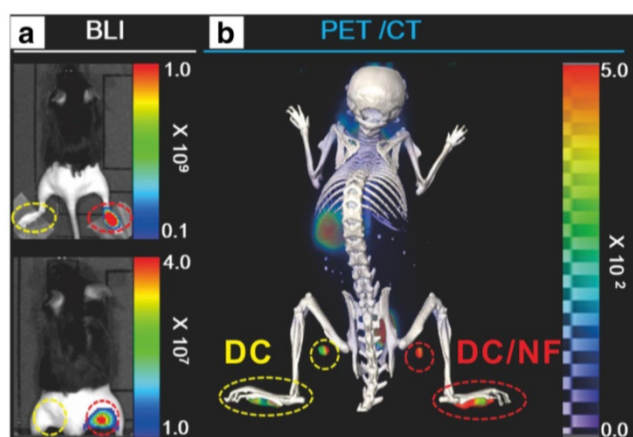


**Figure 9.** In vivo combined bioluminescence (BLI) and [ $^{18}\text{F}$ ]TFB PET/CT imaging of DC migration after their subcutaneous injection into footpads. **(A)** In vivo BLI (upper panel: without masking the footpads; lower panel: after masking the footpads) and **(B)** [ $^{18}\text{F}$ ]TFB PET/CT imaging of DC/NF cell migration to the DPLNs after their injection into mouse footpads. Reproduced with permission from [60], copyright 2017 Springer.

#### 4.2. Preclinical [ $^{18}\text{F}$ ]TFB PET in a pig model

Large animal model investigations with [ $^{18}\text{F}$ ]TFB may take advantage of the accurate quantitation afforded from measured attenuation correction. Hickey et al. [62] reported on the application of [ $^{18}\text{F}$ ]TFB PET/CT imaging as a NIS gene reporter in hepatocyte gene therapy to correct the metabolic disorder in fumarylacetoacetate hydrolase-deficient (Fah $^{-/-}$ ) pigs, a large animal model of hereditary tyrosinemia type 1 (HT1). In this study, hepatocytes were transduced with one or both of the lentiviral vectors expressing the therapeutic Fah and reporter NIS genes, and transplanted into livers of Fah-deficient pigs. As shown in **Figure 11**, higher [ $^{18}\text{F}$ ]TFB uptake was observed in the liver of pig Y842 (denoted in purple) than wide type, which demonstrated near-complete liver repopulation by gene-corrected cells. The results showed that NIS is a suitable noninvasive reporter for future cell transplantation studies. The low uptake of [ $^{18}\text{F}$ ]TFB in normal liver facilitated detection and quantification of low levels of NIS-dependent activity within the NIS transfected therapeutic cells. And the results showed the promising future of using [ $^{18}\text{F}$ ]TFB to monitor NIS gene reporter in hepatocyte gene therapy.

#### 4.3. [ $^{18}\text{F}$ ]TFB PET in non-human primates

Marti-Climent et al. [63] reported the first PET evaluation of [ $^{18}\text{F}$ ]TFB in non-human primates. In this study, whole-body PET imaging was done in two male *Macaca fascicularis* monkeys. [ $^{18}\text{F}$ ]TFB PET images (**Figure 12**) clearly delineated the thyroid with excellent resolution. Following a rapid vascular clearance phase, a great majority of the radiotracer was localized in NIS-expressing organs (thyroid,

salivary glands and stomach) or excreted in the urine. Dosimetry estimates suggested that [ $^{18}\text{F}$ ]TFB delivered an effective dose slightly higher than the dose produced by [ $^{99\text{m}}\text{Tc}$ ]TcO $_4$ , but much lower than that produced by radioiodine in the form of [ $^{131}\text{I}$ ]NaI, [ $^{123}\text{I}$ ]NaI or [ $^{124}\text{I}$ ]NaI. This successful [ $^{18}\text{F}$ ]TFB PET/CT imaging in non-human primates encouraged researchers to pursue the effectiveness and safety evaluations of [ $^{18}\text{F}$ ]TFB in human subjects.

### 5. Clinical evaluation of [ $^{18}\text{F}$ ]TFB

#### 5.1. [ $^{18}\text{F}$ ]TFB PET imaging in healthy human volunteers

Given the excellent properties of [ $^{18}\text{F}$ ]TFB as a NIS imaging radiotracer evidenced in the preclinical studies, further evaluation of [ $^{18}\text{F}$ ]TFB in humans has been initiated. Jiang et al. [20] reported the first [ $^{18}\text{F}$ ]TFB evaluation in 8 healthy human subjects (4 male, 4 female) utilizing the BF $_3$  synthesis method (**Figure 13**). Molar activities of [ $^{18}\text{F}$ ]TFB at injection were approximately 3 GBq/ $\mu\text{mol}$ . Safety, pharmacokinetics, biodistribution, stability and radiation dosimetry of [ $^{18}\text{F}$ ]TFB were assessed by dynamic and whole-body static PET/CT scans over 4 h after intravenous administration. Overall, [ $^{18}\text{F}$ ]TFB administration was well tolerated with no significant findings on vital signs and no clinically meaningful changes in clinical laboratory assays. Uptake of [ $^{18}\text{F}$ ]TFB was observed in well-known NIS-expressing tissues (thyroid, salivary glands and stomach). The left-ventricular blood pool time-activity curves early after injection showed a multiphasic blood clearance of radiotracer with two rapid clearance phases over the first 20 min, followed by a slower clearance phase. HPLC analysis showed excellent tracer in vivo stability in the blood and urine over the length of 4 h study. High uptake in thyroid supports further evaluation of [ $^{18}\text{F}$ ]TFB in thyroid related disorders. Low background uptake in liver, skeletal muscle, cerebral cortex and other low NIS-expressing tissues will allow evaluation of NIS gene expression in these tissues, whereas the few tissues with high uptake (thyroid, salivary glands and stomach) will be disadvantaged for assessing NIS reporter expression.

#### 5.2. [ $^{18}\text{F}$ ]TFB PET imaging in thyroid cancer patients

O'Doherty et al. [21] reported the first [ $^{18}\text{F}$ ]TFB PET imaging results in thyroid cancer patients (**Figure 14**). For this study, [ $^{18}\text{F}$ ]TFB was administrated with molar activities of  $2.6 \pm 1.4$  GBq/ $\mu\text{mol}$  at time of injection. Dynamic whole-body imaging in five patients showed the rapid clearance of radiotracer from the circulation with excellent target-to-

background ratios in NIS-expressing tissues (thyroid, salivary glands, stomach) within 30-45 min post-injection. Thyroid tumor nodules (13-114 mm maximum diameter) were found to be photopenic against the higher background  $[^{18}\text{F}]\text{TfB}$  uptake in normal thyroid, consistent with lower hNIS

expression in differentiated thyroid cancer (DTC) relative to normal thyroid. No significant changes in vital signs or electrocardiograms were observed. Radiation dosimetry estimates were found to be similar as many other fluorine-18 labeled radiotracers.

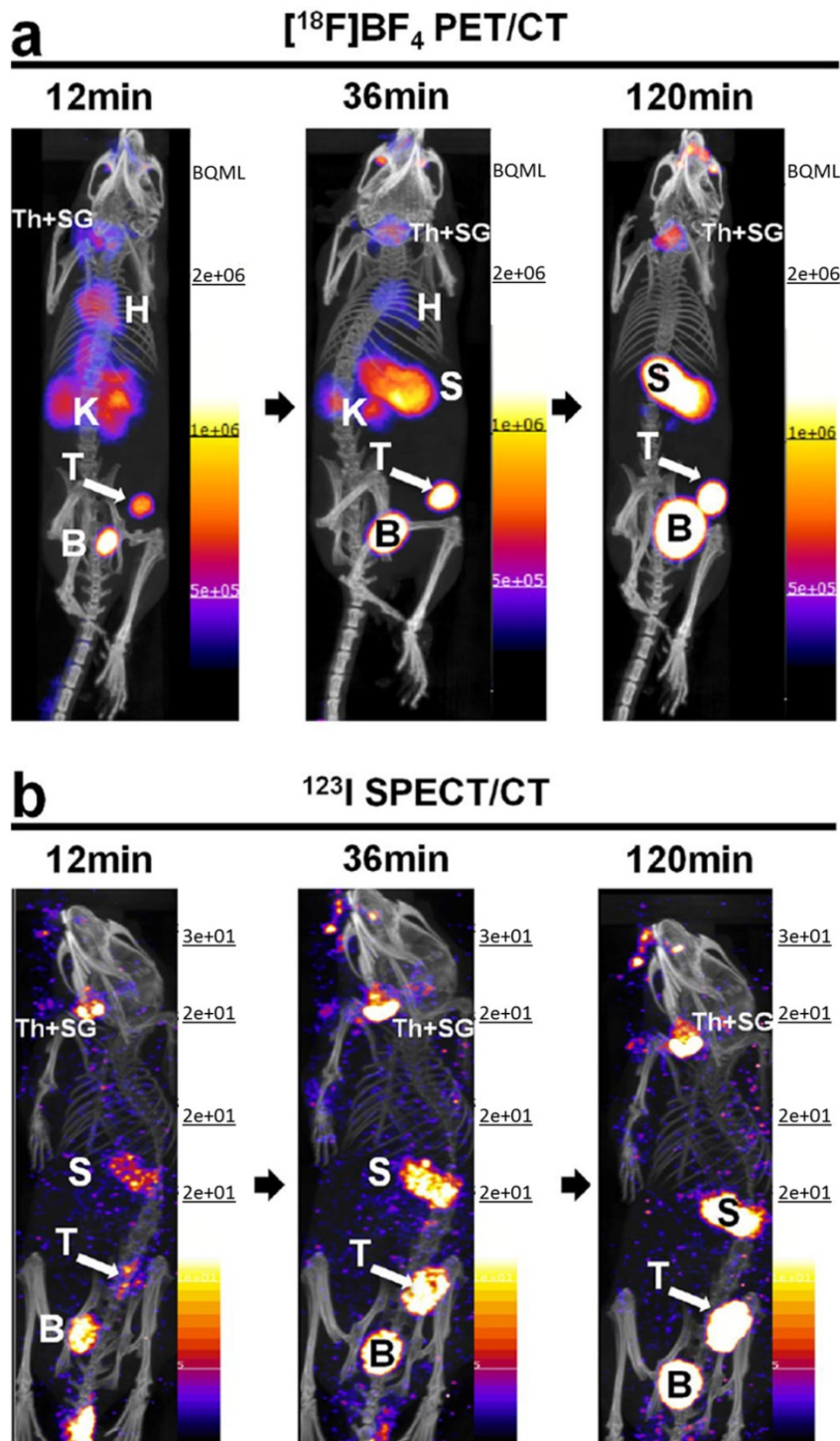


**Figure 10.** Comparative in vivo NIS imaging indicates differences between the PET tracer  $[^{18}\text{F}]\text{TfB}$  and the SPECT tracer  $[^{123}\text{I}]\text{jodide}$ . Tumors were grown to sizes of  $\sim 350 \text{ mm}^3$  before being imaged by either (A)  $[^{18}\text{F}]\text{TfB}$ -PET/CT or (B)  $[^{123}\text{I}]\text{jodide}$ -SPECT/CT. Dynamic PET data were binned into time intervals comparable to sequential SPECT images. All images are maximum intensity projections overlaid on CT. Abbreviations are: bladder (B), heart (H), kidney (K), stomach (S), thyroid and salivary glands (Th + SG), and primary tumor (T). Representative images of cohorts of  $N = 3$  are shown. Reproduced with permission from [61], copyright 2017 Springer Nature.

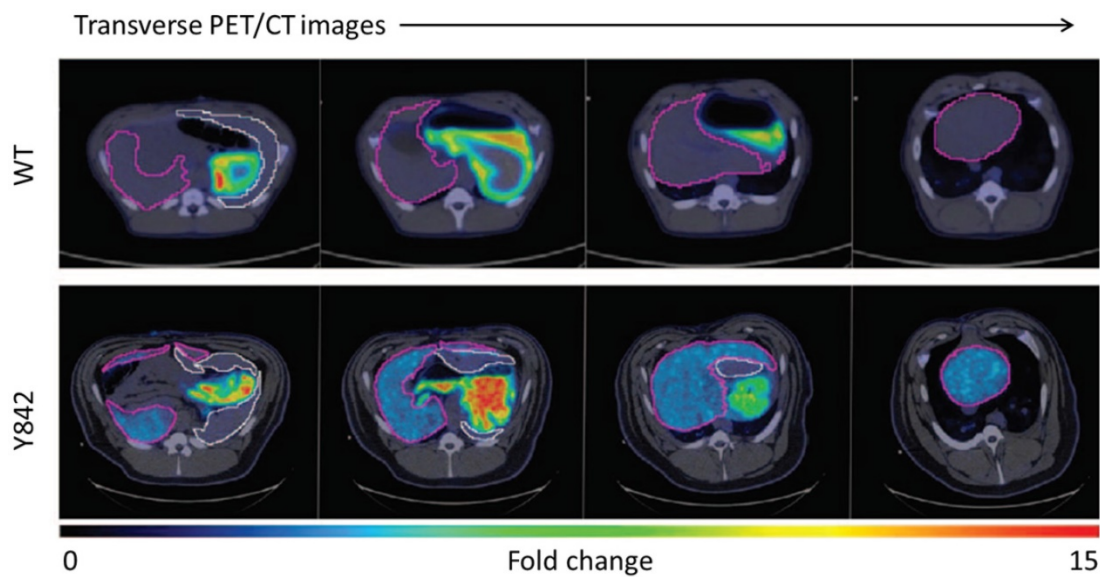


**Figure 11.** Representative transverse PET/CT images of a control WT pig and pig Y842 after injection of [<sup>18</sup>F]TFB. Different positions of the liver are shown from head (left side) to feet (right side) of the animals. The relative intensity of [<sup>18</sup>F]TFB uptake is represented by low (blue) to high (red). The liver is outlined in purple, and the spleen is outlined in white. Reproduced with permission from [62], copyright 2016 Science Translational Medicine, an exclusive license.

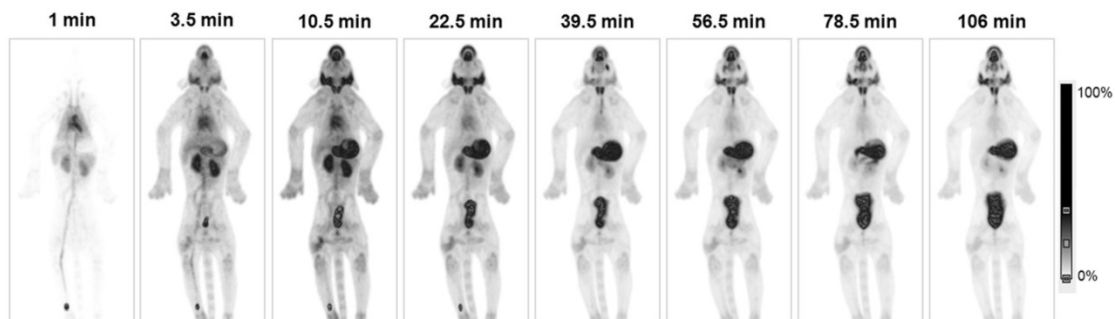


**Figure 12.** [<sup>18</sup>F]TFB biodistribution in macaque. Maximum-intensity projection PET images of the [<sup>18</sup>F]TFB radioactivity at different time points after intravenous injection. Time information corresponds to the mean frame time. Reproduced with permission from [63], copyright 2015 Springer.

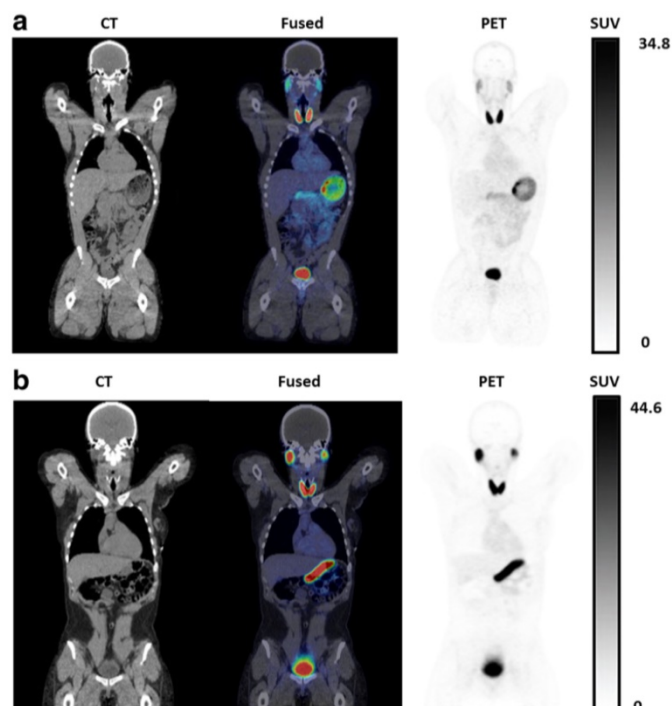


**Figure 13.** Coronal PET/CT images of [<sup>18</sup>F]TFB in healthy (A) male and (B) female participants at 2 h post-injection. Physiologic distribution of [<sup>18</sup>F]TFB is seen in the thyroid, salivary glands, stomach, and intestines. Prominent excretion of radioactivity was seen in the urinary bladder. Reproduced with permission from [20], copyright 2017 Springer.

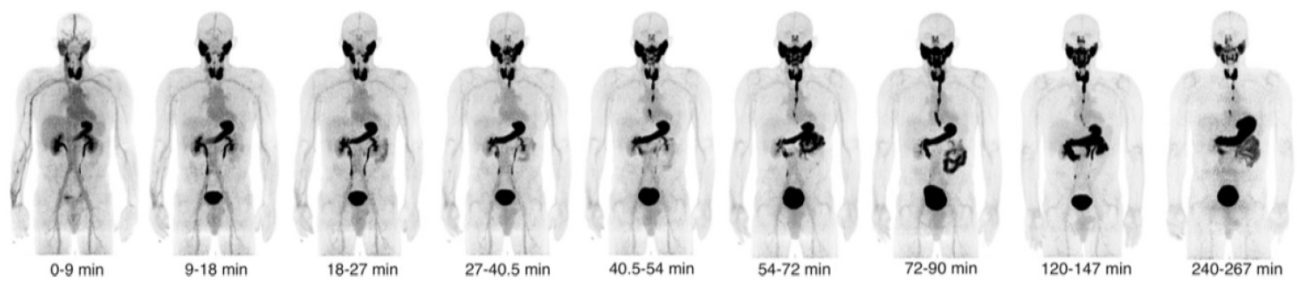


**Figure 14.** Decay-corrected serial maximum-intensity projections showing biodistribution of  $[^{18}\text{F}]\text{TFB}$  over the course of the imaging study. Thyroid, salivary gland, and stomach activities increased rapidly with time up to 30 min. Reproduced with permission from [21], copyright 2017 Society of Nuclear Medicine and Molecular Imaging, Inc.

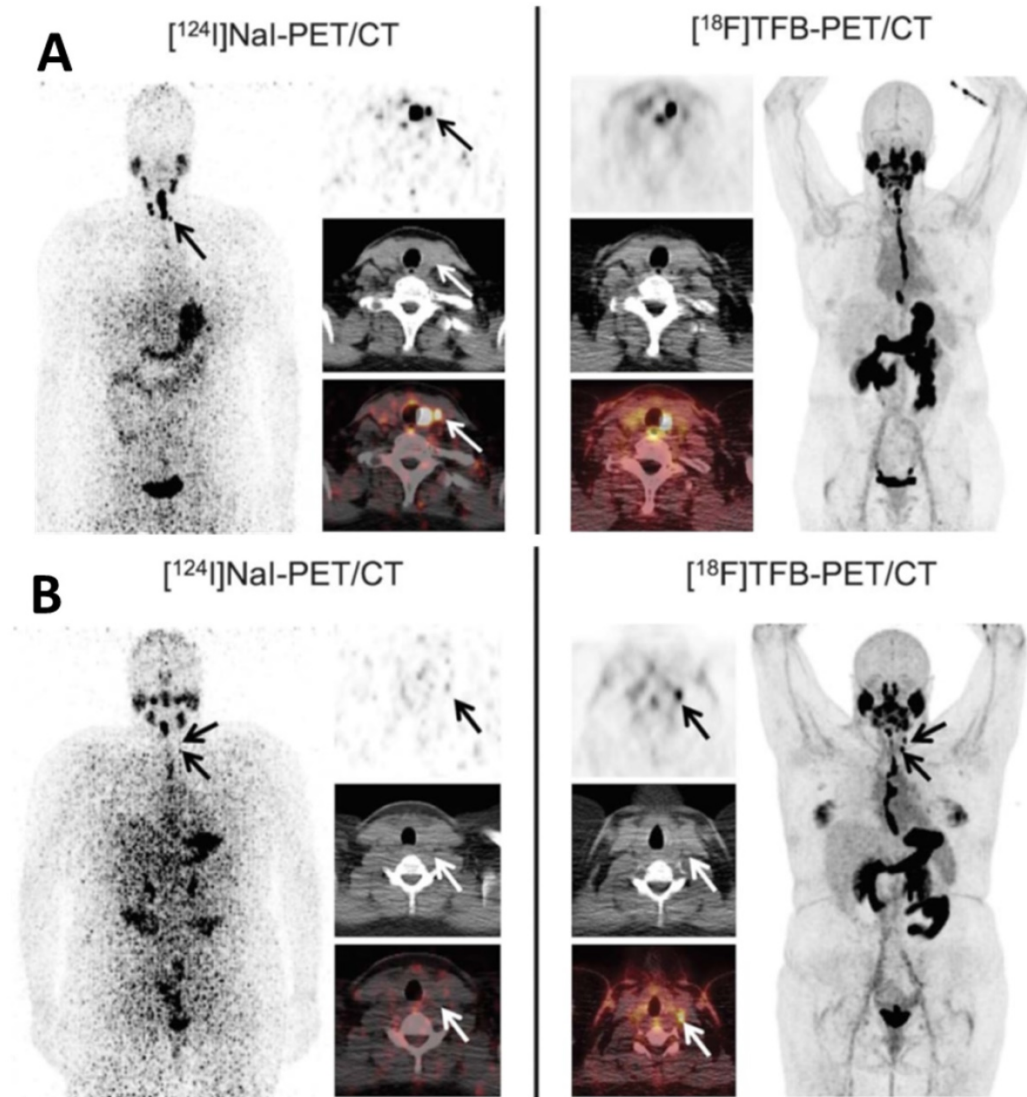


**Figure 15.** Comparison of local thyroid remnant detection by  $[^{18}\text{F}]\text{TFB}$ - and  $[^{124}\text{I}]\text{NaI}$ -PET/CT. Display of maximum intensity projections (outer columns) and transaxial PET and combined PET/CT slices (inner columns). **(A)**  $[^{124}\text{I}]\text{NaI}$ - and  $[^{18}\text{F}]\text{TFB}$ -PET/CT in the 56-year-old patient with DTC presented after total thyroidectomy (pT1b).  $[^{124}\text{I}]\text{NaI}$ - and  $[^{18}\text{F}]\text{TFB}$ -PET/CT revealed remnant benign thyroid tissue in the thyroid bed and along the thyroglossal duct with 2 foci of remnant tissue missed by  $[^{18}\text{F}]\text{TFB}$  (arrows). No lesions suspicious for malignancy were detected. **(B)** Example of a 26-year-old patient after total thyroidectomy with PTC metastases exclusively detected using  $[^{18}\text{F}]\text{TFB}$ -PET/CT. Beside a local thyroid remnant,  $[^{18}\text{F}]\text{TFB}$ -PET/CT confirmed ultrasound results by revealing 2 cervical LNs in the left lateral compartment with focally increased uptake, consistent with metastatic disease (arrows). In contrast,  $[^{124}\text{I}]\text{NaI}$ -PET was unremarkable for malignancy. Because of the discrepant findings, left lateral LN dissection was performed and yielded 6 additional cervical (micro-) metastases. Reproduced with permission from [22], copyright 2018 Wolters Kluwer Health, Inc.

More recently, Samnick et al. [22] reported a comparison study of  $[^{18}\text{F}]\text{TFB}$  and  $[^{124}\text{I}]\text{NaI}$  PET/CT in nine newly diagnosed DTC patients after total thyroidectomy (Figure 15). PET/CT scans were analyzed for the presence of remnant thyroid tissue

and metastatic DTC lesions. Overall, both tracers identified a similar biodistribution pattern and an almost equal number of tumor lesions in a lesion-based analysis ( $[^{18}\text{F}]\text{TFB}$ : 41;  $[^{124}\text{I}]\text{NaI}$ : 40). Retention of iodine-124 in the remnant thyroid tissue

was found to be significantly higher than that of [ $^{18}\text{F}$ ]TFB, which is probably reflective of organification of iodide in thyroid cells. In a single patient, [ $^{18}\text{F}$ ]TFB missed two iodine-124-positive benign thyroid remnants (**Figure 15A**). However, [ $^{18}\text{F}$ ]TFB demonstrated higher accumulation in DTC metastases. For example, [ $^{18}\text{F}$ ]TFB demonstrated additional iodine-124-negative cervical lymph node metastases in 2 patients (**Figure 15B**). The difference in overall agreement between the radiotracers of 91% (74/81 foci) may reflect the aforementioned difference in organification of radioiodine versus lack of organification of [ $^{18}\text{F}$ ]TFB as well as the earlier imaging time point of [ $^{18}\text{F}$ ]TFB (40 min post intravenous administration versus 24 h post oral administration for [ $^{124}\text{I}$ ]NaI). It was concluded that [ $^{18}\text{F}$ ]TFB PET was not inferior to [ $^{124}\text{I}$ ]NaI PET for detecting DTC and its metastases at this point, and may have superiority for detection of [ $^{124}\text{I}$ ]NaI PET-negative metastases in addition to the practical advantages of using a readily synthesized fluorine-18 radiotracer over the less available and more costly iodine-124.

These early human studies show [ $^{18}\text{F}$ ]TFB kinetics and biodistribution to be similar to [ $^{99\text{m}}\text{Tc}$ ]TcO<sub>4</sub>, and that it exhibits higher accumulation in differentiated thyroid cancer metastases [22]. In this regard, [ $^{18}\text{F}$ ]TFB may be favorable to radioiodide for clinical assessments by PET imaging of NIS expression in thyroid-related disorders. The safety assessments of [ $^{18}\text{F}$ ]TFB have shown it to be pharmacologically safe in humans, and radiation dosimetry is on par with other greatly excreted fluorine-18-labeled radiopharmaceuticals, such as [ $^{18}\text{F}$ ]FDG. These results warrant further Phase 2 trials for [ $^{18}\text{F}$ ]TFB as a NIS imaging probe. Indeed, another study of [ $^{18}\text{F}$ ]TFB PET imaging with thyroid cancer patients has been initiated by Memorial Sloan Kettering Cancer Center [64]. There are ongoing studies at Mayo Clinic to perform [ $^{18}\text{F}$ ]TFB imaging in cancer patients undergoing treatment with oncoviruses engineered to express the NIS reporter [65]. These phase 2 trials are necessary to support future regulatory submissions on the use of NIS reporter gene in virotherapy.

With regard to the dependence of [ $^{18}\text{F}$ ]TFB imaging characteristics on molar activity, more data is required in humans to understand this relationship. As noted, the previously discussed studies used preparations that resulted in human administration of [ $^{18}\text{F}$ ]TFB at similar molar activities of approximately 3 GBq/ $\mu\text{mol}$  [20, 21]. This level of molar activity is achievable with the isotope-exchange method or BF<sub>3</sub>-based radiosynthesis methods, although in our hands, we are able to achieve ~2-fold higher

radiochemical yields and ~5-fold higher molar activities with the BF<sub>3</sub>-based method, which may allow for longer delays between end of synthesis and radiotracer administration. Obviously, further work is required to define recommended minimum molar activity levels to avoid saturation effects at NIS transporters and maintain target-to-background characteristics.

## 6. Conclusion and perspectives

NIS has been extensively evaluated as a target for therapy and reporter gene in the last two decades after the cloning of the NIS gene. The introduction of [ $^{18}\text{F}$ ]TFB for PET imaging of NIS-expressing tissues may allow imaging assessments to be improved over conventional imaging with SPECT or PET iodide probes. The simple synthesis methods established for preparation of [ $^{18}\text{F}$ ]TFB are amenable for production in existing medical cyclotron facilities and fluorine-18 radiopharmaceutical distribution centers. [ $^{18}\text{F}$ ]TFB may have limited availability in medical centers not equipped with a medical cyclotron. However, this should not be a big concern because a distribution approach can solve this problem owing to the favorable half-life of 109.8 min, and this distribution model has been proven to be very successful with [ $^{18}\text{F}$ ]FDG. In light of its excellent preclinical and preliminary clinical evaluations, we can expect that translational studies with [ $^{18}\text{F}$ ]TFB will continue to improve the further advancement of NIS imaging in thyroid disorders (e.g., differentiated thyroid cancer and metastasis of thyroid cancer) and NIS reporter gene imaging (e.g., viral-mediated gene therapy, oncolytic viral therapy and cell trafficking). The excellent results in recent clinical studies also imply that [ $^{18}\text{F}$ ]TFB has the potential to offer alternative options to [ $^{99\text{m}}\text{Tc}$ ]TcO<sub>4</sub> or radioiodides for clinical NIS imaging using SPECT and PET. Thus, [ $^{18}\text{F}$ ]TFB and closely related compounds under investigation have the potential to expand the role of NIS in nuclear radiology in the future.

## Abbreviations

BF<sub>3</sub>: boron trifluoride; CT: computed tomography; DC: dendritic cell; DPLNs: draining popliteal lymph nodes; DTC: differentiated thyroid cancer; EOS: end of synthesis; FDG: fludeoxyglucose; FSO<sub>3</sub>: fluorosulfate; GMP: good manufacturing practices; I: iodide; K.2.2.2: Kryptofix® 2.2.2; MV: measles virus; NIS: sodium/iodide symporter; NMP: N-methylpyrrolidine; PET: positron emission tomography; PF<sub>6</sub>: hexafluorophosphate; QMA: quaternary methyl ammonium; SPECT: single photon emission computed tomography; TcO<sub>4</sub>: pertechnetate; TFB: tetrafluoroborate.

## Acknowledgements

This work was supported by the NIH/NCI CA196975-01.

## Competing Interests

The authors have declared that no competing interest exists.

## References

- Maxon HR, Thomas SR, Hertzberg VS, Kereiakes JG, Chen IW, Sperling MI, et al. Relation between effective radiation dose and outcome of radioiodine therapy for thyroid cancer. *N Engl J Med.* 1983; 309: 937-41.
- Bartalena L, Marcocci C, Bogazzi F, Panicucci M, Lepri A, Pinchera A. Use of corticosteroids to prevent progression of Graves' ophthalmopathy after radioiodine therapy for hyperthyroidism. *N Engl J Med.* 1989; 321: 1349-52.
- Franklyn JA, Maisonneuve P, Sheppard M, Betteridge J, Boyle P. Cancer incidence and mortality after radioiodine treatment for hyperthyroidism: a population-based cohort study. *The Lancet.* 1999; 353: 2111-5.
- Chung JK. Sodium iodide symporter: its role in nuclear medicine. *J Nucl Med.* 2002; 43: 1188-200.
- Ahn BC. Sodium iodide symporter for nuclear molecular imaging and gene therapy: from bedside to bench and back. *Theranostics.* 2012; 2: 392-402.
- Durante C, Haddy N, Baudin E, Leboulleux S, Hartl D, Travagli J, et al. Long-term outcome of 444 patients with distant metastases from papillary and follicular thyroid carcinoma: benefits and limits of radioiodine therapy. *J Clin Endocrinol Metab.* 2006; 91: 2892-9.
- Luster M, Clarke S, Dietlein M, Lassmann M, Lind P, Oyen W, et al. Guidelines for radioiodine therapy of differentiated thyroid cancer. *Eur J Nucl Med Mol Imag.* 2008; 35: 1941-59.
- Hänscheid H, Lassmann M, Luster M, Thomas SR, Pacini F, Ceccarelli C, et al. Iodine biokinetics and dosimetry in radioiodine therapy of thyroid cancer: procedures and results of a prospective international controlled study of ablation after rhTSH or hormone withdrawal. *J Nucl Med.* 2006; 47: 648-54.
- Dai G, Levy O, Carrasco N. Cloning and characterization of the thyroid iodide transporter. *Nature.* 1996; 379: 458-60.
- Smanik PA, Liu Q, Furminger TL, Ryu K, Xing S, Mazzaferri EL, et al. Cloning of the human sodium iodide symporter. *Biochem Biophys Res Commun.* 1996; 226: 339-45.
- Portulano C, Paroder-Belenitsky M, Carrasco N. The Na<sup>+</sup>/I<sup>-</sup> symporter (NIS): mechanism and medical impact. *Endocr Rev.* 2014; 35: 106-49.
- Cavalieri RR. Iodine metabolism and thyroid physiology: current concepts. *Thyroid.* 1997; 7: 177-81.
- Shah K, Jacobs A, Breakefield XO, Weissleder R. Molecular imaging of gene therapy for cancer. *Gene Ther.* 2004; 11: 1175-87.
- Spitzweg C, Harrington KJ, Pinke LA, Vile RG, Morris JC. The sodium iodide symporter and its potential role in cancer therapy. *J Clin Endocrinol Metab.* 2001; 86: 3327-35.
- Penheiter AR, Russell SJ, Carlson SK. The sodium iodide symporter (NIS) as an imaging reporter for gene, viral, and cell-based therapies. *Curr Gene Ther.* 2012; 12: 33-47.
- Serganova I, Ponomarev V, Blasberg R. Human reporter genes: potential use in clinical studies. *Nucl Med Biol.* 2007; 34: 791-807.
- Kang JH, Chung JK. Molecular-genetic imaging based on reporter gene expression. *J Nucl Med.* 2008; 49 (Suppl 2): 164S-79.
- Kang JH, Lee DS, Paeng JC, Lee JS, Kim YH, Lee YJ, et al. Development of a sodium/iodide symporter (NIS)-transgenic mouse for imaging of cardiomyocyte-specific reporter gene expression. *J Nucl Med.* 2005; 46: 479-83.
- Jauregui-Osoro M, Sunassee K, Weeks AJ, Berry DJ, Paul RL, Cleij M, et al. Synthesis and biological evaluation of [<sup>18</sup>F]tetrafluoroborate: a PET imaging agent for thyroid disease and reporter gene imaging of the sodium/iodide symporter. *Eur J Nucl Med Mol Imag.* 2010; 37: 2108-16.
- Jiang H, Schmit NR, Koenen AR, Bansal A, Pandey MK, Glynn RB, et al. Safety, pharmacokinetics, metabolism and radiation dosimetry of [<sup>18</sup>F]tetrafluoroborate ([<sup>18</sup>F]TFB) in healthy human subjects. *EJNMMI Res.* 2017; 7: 90.
- O' Doherty J, Jauregui-Osoro M, Brothwood T, Szyszko T, Marsden P, O' Doherty M, et al. [<sup>18</sup>F]tetrafluoroborate ([<sup>18</sup>F]TFB), a PET probe for imaging sodium-iodide symporter expression: Whole-body biodistribution, safety and radiation dosimetry in thyroid cancer patients. *J Nucl Med.* 2017; 58: 1666-71.
- Samnack S, Al-Momani E, Schmid J-S, Mottok A, Buck AK, Lapa C. Initial Clinical Investigation of [<sup>18</sup>F]Tetrafluoroborate PET/CT in Comparison to [<sup>124</sup>I]Iodine PET/CT for Imaging Thyroid Cancer. *Clin Nucl Med.* 2018; 43: 162-7.
- Bar-Shalom R, Yefremov N, Guralnik L, Gaitini D, Frenkel A, Kuten A, et al. Clinical performance of PET/CT in evaluation of cancer: additional value for diagnostic imaging and patient management. *J Nucl Med.* 2003; 44: 1200-9.
- Schütz F, Lautenschläger C, Lorenz K, Haerting J. Positron emission tomography (PET) and PET/CT in thyroid cancer: a systematic review and meta-analysis. *Eur. Thyroid. J.* 2018; 7: 13-20.
- Beyer T, Townsend DW, Brun T, Kinahan PE. A combined PET/CT scanner for clinical oncology. *J Nucl Med.* 2000; 41: 1369-79.
- Blodgett TM, Meltzer CC, Townsend DW. PET/CT: form and function. *Radiology.* 2007; 242: 360-85.
- Weber DA, Ivanovic M, Franceschi D, Strand S, Erlandsson K, Franceschi M, et al. Pinhole SPECT: an approach to in vivo high resolution SPECT imaging in small laboratory animals. *J Nucl Med.* 1994; 35: 342-8.
- Sparagana M, Little A, Kaplan E. Rapid evaluation of thyroid nodules using [<sup>99m</sup>Tc]pertechnetate scanning. *J Nucl Med.* 1970; 11: 224-5.
- Frans JT, Berman DS, Maddahi J, Watson DD, Beller GA, Strauss HW, et al. Technetium-99m hexakis 2-methoxyisobutyl isonitrile: human biodistribution, dosimetry, safety, and preliminary comparison to thallium-201 for myocardial perfusion imaging. *J Nucl Med.* 1989; 30: 301-11.
- Boyd R. Molybdenum-99: technetium-99m generator. *Radiochimica acta.* 1982; 30: 123-45.
- Ruth T. Accelerating production of medical isotopes. *Nature.* 2009; 457: 536-7.
- Pillai MRA, Knapp FF. Overcoming the Tc-99m Shortage: Are Options Being Overlooked? *J Nucl Med.* 2011; 52 (No 2): 15N-28.
- Filzen LM, Ellingson LR, Paulsen AM, Hung JC. Potential ways to address shortage situations of <sup>99</sup>Mo/<sup>99m</sup>Tc. *J Nucl Med Technol.* 2017; 45: 1-5.
- Hill TC, Holman BL, Lovett R, O'Leary DH, Magistretti P, Zimmerman RE, et al. Initial experience with SPECT (single-photon computerized tomography) of the brain using N-isopropyl I-123 p-iodoamphetamine: concise communication. *J Nucl Med.* 1982; 23: 191-5.
- King MA, Schwinger RB, Penney BC, Doherty PW, Bianco JA. Digital restoration of indium-111 and iodine-123 SPECT images with optimized Metz filters. *J Nucl Med.* 1986; 27: 1327-36.
- Iida H, Itoh H, Nakazawa M, Hatazawa J, Nishimura H, Onishi Y, et al. Quantitative mapping of regional cerebral blood flow using iodine-123-IMP and SPECT. *J Nucl Med.* 1994; 35: 2019-30.
- Ryo UY, Vaidya PV, Schneider AB, Bekerman C, Pinsky SM. Thyroid imaging agents: a comparison of I-123 and Tc-99m pertechnetate. *Radiology.* 1983; 148: 819-22.
- Kim EM, Park EH, Cheong SJ, Lee CM, Kim DW, Jeong HJ, et al. Characterization, biodistribution and small-animal SPECT of I-125-labeled c-Met binding peptide in mice bearing c-Met receptor tyrosine kinase-positive tumor xenografts. *Nucl Med Biol.* 2009; 36: 371-8.
- Qiu ZI, Luo QY. Erector spinae metastases from differentiated thyroid cancer identified by I-131 SPECT/CT. *Clin Nucl Med.* 2009; 34: 137-40.
- Macdonald W, Armstrong J. Benign struma ovarii in a patient with invasive papillary thyroid cancer: detection with I-131 SPECT-CT. *Clin Nucl Med.* 2007; 32: 380-2.
- Tharp K, Israel O, Hausmann J, Bettman L, Martin W, Daitzchman M, et al. Impact of <sup>131</sup>I-SPECT/CT images obtained with an integrated system in the follow-up of patients with thyroid carcinoma. *Eur J Nucl Med Mol Imag.* 2004; 31: 1435-42.
- Čomor J, Stevanović Ž, Rajčević M, Košutić D. Modeling of thermal properties of a TeO<sub>2</sub> target for radioiodine production. *Nucl Instr Meth Phys Res. A.* 2004; 521: 161-70.
- Eschmann SM, Reischl G, Bilger K, Kupferschläger J, Thelen MH, Dohmen BM, et al. Evaluation of dosimetry of radioiodine therapy in benign and malignant thyroid disorders by means of iodine-124 and PET. *Eur J Nucl Med Mol Imag.* 2002; 29: 760-7.
- Phan HT, Jager PL, Paans AM, Plukker JT, Sturkenboom MG, Sluiter WJ, et al. The diagnostic value of <sup>124</sup>I-PET in patients with differentiated thyroid cancer. *Eur J Nucl Med Mol Imag.* 2008; 35: 958-65.
- Pentlow KS, Graham MC, Lambrecht RM, Daghighian F, Bacharach SL, Bendriem B, et al. Quantitative Imaging of Iodine-124 with PET. *J Nucl Med.* 1996; 37: 1557-62.
- Blau M, Nagler W, Bender M. Fluorine-18: a new isotope for bone scanning. *J Nucl Med.* 1962; 3: 332-4.
- Anbar M, Guttman S, Lewitus Z. Effect of monofluorosulphonate, difluorophosphate and fluoroborate ions on the iodine uptake of the thyroid gland. *Nature.* 1959; 183: 1517-8.
- Anbar M, Guttman S, Lewitus Z. The accumulation of fluoroborate ions in thyroid glands of RatS1. *Endocrinology.* 1960; 66: 888-90.
- Anbar M, Guttman S. The isotopic exchange of fluoroboric acid with hydrofluoric acid. *The J Phys Chem.* 1960; 64: 1896-9.
- Khoshnevisan A, Chuamsaamarkkee K, Boudjemline M, Jackson A, Smith GE, Gee AD, et al. [<sup>18</sup>F]fluorosulfate for pet imaging of the sodium-iodide symporter: synthesis and biologic evaluation in vitro and in vivo. *J Nucl Med.* 2017; 58: 156-61.
- Waltz F, Pilette L, Ambroise Y. A nonradioactive iodide uptake assay for sodium iodide symporter function. *Anal Biochem.* 2010; 396: 91-5.
- Youn H, Jeong JM, Chung JK. A new PET probe, [<sup>18</sup>F]tetrafluoroborate, for the sodium/iodide symporter: possible impacts on nuclear medicine. *Eur J Nucl Med Mol Imag.* 2010; 37: 2105-7.
- Jiang H, Bansal A, Pandey MK, Peng KW, Suksanpaisan L, Russell SJ, et al. Synthesis of [<sup>18</sup>F]tetrafluoroborate via radiofluorination of boron trifluoride and evaluation in a murine C6-glioma tumor model. *J Nucl Med.* 2016; 57: 1454-9.
- Khoshnevisan A, Jauregui-Osoro M, Shaw K, Torres JB, Young JD, Ramakrishnan NK, et al. [<sup>18</sup>F]tetrafluoroborate as a PET tracer for the sodium/iodide symporter: the importance of specific activity. *EJNMMI Res.* 2016; 6: 34.

55. Volpe A, Man FA, Lim LY, Khoshnevisan A, Blower JE, Blower PJ, et al. Radionuclide-fluorescence reporter gene imaging to track tumor progression in rodent tumor models. *J Vis Exp*. 2018; 133.
56. Weeks AJ, Jauregui-Osoro M, Cleij M, Blower JE, Ballinger JR, Blower PJ. Evaluation of [<sup>18</sup>F]tetrafluoroborate as a potential PET imaging agent for the human sodium/iodide symporter in a new colon carcinoma cell line, HCT116, expressing hNIS. *Nucl Med Commun*. 2011; 32: 98-105.
57. Jiang H, Bansal A, Goyal R, Peng KW, Russell SJ, DeGrado TR. Synthesis and evaluation of [<sup>18</sup>F]hexafluorophosphate as a novel PET probe for imaging of sodium/iodide symporter in a murine C6-glioma tumor model. *Bioorganic Med. Chem*. 2018; 26: 225-31.
58. Domingo-Musibay E, Allen C, Kurokawa C, Hardcastle JJ, Aderca I, Msaouel P, et al. Measles Edmonston vaccine strain derivatives have potent oncolytic activity against osteosarcoma. *Cancer Gene Ther*. 2014; 21: 483-90.
59. Lee HW, Yoon SY, Singh TD, Choi YJ, Lee HJ, Park JY, et al. Tracking of dendritic cell migration into lymph nodes using molecular imaging with sodium iodide symporter and enhanced firefly luciferase genes. *Sci Rep*. 2015; 5: 9865.
60. Lee SB, Lee HW, Lee H, Jeon YH, Lee SW, Ahn BC, et al. Tracking dendritic cell migration into lymph nodes by using a novel PET probe [<sup>18</sup>F]tetrafluoroborate for sodium/iodide symporter. *EJNMMI Res*. 2017; 7: 32.
61. Diocou S, Volpe A, Jauregui-Osoro M, Boudjemeline M, Chuamsaamarkkee K, Man F, et al. [<sup>18</sup>F] tetrafluoroborate-PET/CT enables sensitive tumor and metastasis in vivo imaging in a sodium iodide symporter-expressing tumor model. *Sci Rep*. 2017; 7: 946.
62. Hickey RD, Mao SA, Glorioso J, Elgilani F, Amiot B, Chen H, et al. Curative ex vivo liver-directed gene therapy in a pig model of hereditary tyrosinemia type 1. *Sci Transl Med*. 2016; 8: 349ra99.
63. Marti-Climent JM, Collantes M, Jauregui-Osoro M, Quincoces G, Prieto E, Bilbao I, et al. Radiation dosimetry and biodistribution in non-human primates of the sodium/iodide PET ligand [<sup>18</sup>F]tetrafluoroborate. *EJNMMI Res*. 2015; 5:70.
64. [Internet] Study of PET Imaging With [<sup>18</sup>F]IFB in Patients With Thyroid Cancer. June 22, 2017 first posted. <https://clinicaltrials.gov/ct2/show/NCT03196518>.
65. [Internet] PET (Positron Emission Tomography) Imaging Studies With NIS Reporter. September 20, 2016. <https://clinicaltrials.gov/ct2/show/NCT02907073>.